very low in amplitude, casts doubt on the suggestion that the free-radical pathway is the most important route for the control of the oscillations.

It is not possible to propose a model for the findings reported here, until more careful measurements are carried out with different concentrations of the reactants.

*Acknowledgment.* We thank Ms. Merete Torpe for help in carrying out the measurements and Dr. Erik Pedersen for collaboration and assistance in the ESR instrumentation. B.V. expresses his thanks to the Danish Research Academy and Professor Thor A. Bak for making it possible to avail of a visiting professorship at the Ørsted Institute.

# Ultrafast Measurements on Direct Photoinduced Electron Transfer in a Mixed-Valence Complex

**Gilbert C. Walker, Paul F. Barbara,***

*Department of Chemistry, University of Minnesota, Minneapolis, Minnesota 55455*

**Stephen K. Doorn, Yuhua Dong, and Joseph T. Hupp**

*Department of Chemistry, Northwestern University, Evanston, Illinois 60208* *(Received: May 1, 1991; In Final Form: June 6, 1991)*

A direct measurement of the kinetics of intramolecular photoinduced metal-metal charge transfer has been made, i.e.

$$(NH_3)_5Ru^{III}NCFe^{II}(CN)_5^- \underset{k_{ET}}{\overset{h\nu}{\rightleftharpoons}} (NH_3)_5Ru^{II}NCFe^{III}(CN)_5^-$$

where the solvent is $H_2O$ or $D_2O$ and $k_{ET}$ signifies the reverse-electron-transfer (ET) rate coefficient. The apparent reverse-electron-transfer kinetics are nonexponential with a limiting rate constant, $k_{lim} = k(t)$ where $t \rightarrow \infty$, equal to $(8 \pm 3) \times 10^{11}$ s$^{-1}$. This is close to the theoretical predictions from the model of Sumi and Marcus (classical vibrational modes), $k_{ET,SM} = 10^{13}$ and $5 \times 10^{12}$ s$^{-1}$, and from the model of Jortner and Bixon (quantum mechanical vibrations), $k_{ET,JB} = 1.2 \times 10^{12}$ s$^{-1}$. The parameters required for these theories were estimated by resonance Raman spectroscopy, static absorption spectroscopy, and recently published transient Stokes shift measurements.

## Introduction

Compounds exhibiting mixed-valence metal-metal charge-transfer transitions (MMCT)[1] have played a central role in the development of the understanding of electron-transfer (ET) reactions. In Marcus's theory of ET,[2] the energy of the absorption maximum $h\nu_{max}$ gives direct information on the reorganization energy $\lambda$, as follows

$$h\nu_{max} = \lambda + \Delta G^\circ \quad (1)$$

where $h$ is Planck's constant and $\Delta G^\circ$ is the driving force, as shown in Figure 1, which represents the reaction described in this paper.

The MMCT absorption band also gives a measure of a key ET parameter, the electronic matrix element, $V_{el}$.[3] Resonance Raman spectroscopy on the MMCT band gives detailed information on the vibrational modes that are coupled to the ET reaction.[4] Two additional types of data are needed for an "absolute" rate prediction, namely, a measure of the dynamics of the solvent coordinate and a measure of the reaction driving force $\Delta G^\circ$. For a typical MMCT compound, such as in Figure 1, $\Delta G^\circ$ can be approximately estimated from redox potential of the isolated metal systems or other methods. Estimates for the required solvation dynamical information are available from recent transient Stokes shift measurements on polar fluorescent probes.[5] In summary, all the parameters that are necessary to make a prediction of the ET rate constant, $k_{ET}$, for MMCT compounds can be experimentally obtained, but no such comparison has been reported to our knowledge.

In this paper, we report the first direct kinetic measurement of a MMCT optically induced ET reaction, as represented in Figure 1, and compare the experimental results to theoretical predictions using experimentally estimated parameters. It should be noted that a report has appeared in which MMCT kinetics were indirectly induced by metal-ligand charge-transfer optical excitation.[6] Our work is oriented, in part, toward evaluating contemporary theoretical models that explicitly consider the dramatic effect of solvation dynamics on ET rates.[7] In the past decade it has been established that ET rates can be directly proportional to the time scale for solvent motion for simple systems in certain limits, i.e.

$$k_{ET} \simeq \tau_s^{-1} \exp(-\Delta G/k_bT) \quad (2)$$

Thus for small barrier reactions ($\Delta G \ll k_bT$) $k_{ET}$ is solvent controlled, i.e., $k_{ET} \simeq \tau_s^{-1}$. We are particularly concerned in this paper with obtaining experimental evidence on how the simple picture of eq 2 is affected by strong electronic coupling, vibrational modes, and frequency-dependent solvent friction effects.[7]

## Experimental Methods

The transient pump-probe apparatus has been described elsewhere.[8] The laser source is an intermediate repetition rate (8.2 kHz) amplified dye laser ($\lambda$ = 792 nm) with 70-fs pulse duration. The energies of the pump and probe pulses were typically 400 and 20 nJ, respectively. The spot sizes were $\simeq$100 $\mu$m. The continuum light probe pulses were generated in water or a

* To whom correspondence should be addressed.

(1) Creutz, C. *Prog. Inorg. Chem.* **1983**, *30*, 1.
(2) Marcus, R. A. *Annu. Rev. Phys. Chem.* **1964**, *15*, 155. Marcus, R. A.; Sutin, N. *Biochim. Phys. Acta* **1985**, *811*, 265.
(3) Hush, N. S. *Prog. Inorg. Chem.* **1967**, *8*, 391.
(4) Doorn, S. K.; Hupp, J. T. *J. Am. Chem. Soc.* **1990**, *112*, 4999. Doorn, S. K.; Hupp, J. T. *J. Am. Chem. Soc.* **1990**, *112*, 1142.
(5) Walker, G. C.; Jarzeba, W.; Johnson, A. E.; Kang, T. J.; Barbara, P. F. *J. Opt. Soc. Am. B* **1990**, *7*, 1521. Walker, G. C.; Jarzeba, W.; Johnson, A. E.; Barbara, P. F. Manuscript in preparation.
(6) Creutz, C.; Krofer, P.; Matsubara, T.; Netzel, T. L.; Sutin, N. *J. Am. Chem. Soc.* **1979**, *101*, 5442.
(7) For recent reviews on dynamic solvent effects on ET kinetics, see: Barbara, P. F.; Jarzeba, W. *Adv. Photochem.* **1990**, *15*, 1. Maroncelli, M.; MacInnis, J.; Fleming, G. R. *Science* **1989**, *243*, 1674. Simon, J. D. *Acc. Chem. Res.* **1988**, *21*, 128. Weaver, M. J.; McManis III, G. E. *Acc. Chem. Res.* **1990**, *34*, 294.
(8) Åkesson, E.; Walker, G. C.; Barbara, P. F. *J. Chem. Phys.*, in press. Kahlow, M. J.; Jarzeba, W.; DuBruil, T. P.; Barbara, P. F. *Rev. Sci. Instrum.* **1988**, *59*, 1098.

0022-3654/91/2095-5712$02.50/0 

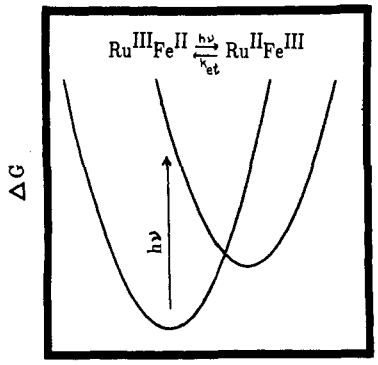


**Figure 1.** $Ru^{III}Fe^{II}$ (left) and $Ru^{II}Fe^{III}$ (right) free energy surfaces generated using a classical model for all of the reorganization energy. In a schematic description, the pump laser (792 nm) induces direct, optical electron transfer (the vertical arrow) and the reverse-electron-transfer rate (which might occur as schematically shown by the downward arrows) is measured by optically probing the recovery of the initial population.

mixture of water and ethylene glycol. The general synthetic procedure of Vogler and Kisslinger[9] was used to prepare $(NH_3)_5Ru^{III}NCFe^{II}(CN)_5^-$, except that samples were further purified by passage through a DOWEX 50WX8 cation-exchange column. Sample concentrations were typically $5 \times 10^{-3}$ M.

## Results and Discussion

**Static Spectroscopy.** We have recorded transient pump–probe spectroscopy of the MMCT transition (Figure 1) of $(NH_3)_5Ru^{III}NCFe^{II}(CN)_5^-$. The MMCT band of $Ru^{III}Fe^{II}$ in water is peaked at 10 200 $cm^{-1}$ (975 nm) and has a bandwidth of 4900 $cm^{-1}$. It is not overlapped by any other observable optical transition of $Ru^{III}Fe^{II}$. The molar extinction coefficient of the MMCT band, $\epsilon_{max} = 3000\ cm^{-1}$, and the bandwidth can be used to estimate the electronic matrix element, $V_{el}$.[3,10] The estimated value (1500 $cm^{-1}$)[10] is large and is indicative of a relatively strong metal-metal interaction due to the short metal–metal distance and the interaction provided by the cyanide bridging ligand.

The photon energy that corresponds to the frequency of the peak of the absorption spectrum, $h\nu_{max}$, gives an estimate of the total reorganization energy

$$\lambda \equiv h\nu_{max} - \Delta G^\circ \simeq \lambda_{class} + \lambda_{QM} \qquad (3)$$

where $\lambda_{class}$ and $\lambda_{QM}$ are the low-frequency (classical) and high-frequency (quantum mechanical) contributions to the total reorganization energy, and $\Delta G^\circ$ is the driving force[11] of the ET. Equation 3 is an approximation that is valid when the solvent broadening is strong enough to ensure a structureless band; see ref 12.

**TABLE I: Structural and Franck–Condon Charge-Transfer Parameters for $(NH_3)_5Ru$–NC–$Fe(CN)_5^-$ from Postresonance Raman ($\lambda_{exc}$ = 647.1 nm)**

| band, $cm^{-1}$ | assignment | $I_{rel}$[a,b] | $\lvert\Delta a\rvert$,[b-d] Å | $\lambda'_{vib}$,[b-e] $cm^{-1}$ |
|---|---|---|---|---|
| 2104 | $\nu_{C\equiv N,bridge}$ | 15 | 0.045 | 870 |
| 2060 | $\nu_{C\equiv N,term}$ | 1.3 | 0.0069 | 80 |
| 603 | $\nu_{Fe-C,bridge}$ | 4.1 | 0.039 | 830 |
| 544 | $\nu_{Fe-C,term}$ | 0.92 | 0.043 | 210 |
| 482 | $\nu_{Ru-NH_3}$ | 1.0 | 0.034 | 250 |
| 468 | $\nu_{Ru-NH_3,axial}$ | 0.53 | 0.052 | 140 |
| 361 | $\nu_{Ru-NC}$ | 0.34 | 0.049 | 120 |
| 270 | $\delta_{H_3N-Ru-NH_3}$ | 1.6 | | 720 |

[a] Relative Raman scattering intensity; all modes are resonantly enhanced. [b] Raman data were obtained at postresonance. Detailed spectral simulations suggest that some minor reordering of relative scattering intensities (and therefore $|\Delta a|$ and $\lambda'_{vib}$ values) will be observed when experiments are performed at preresonance. The simulations also suggest that the most accurate structural parameters will be obtained at preresonance. [c] A description for the derivation of these values may be found in ref 4. The value of $\sigma$ used in this calculation was 1740 $cm^{-1}$. Solvent reorganization was assumed *not* to contribute to the overall breadth of the absorption band, adding breadth instead only to the individual vibrational components. [d] Absolute bond length displacements following electron transfer; derived values are based on a local mode approximation (see ref 4). [e] Single mode contribution to the total vibrational reorganization energy.

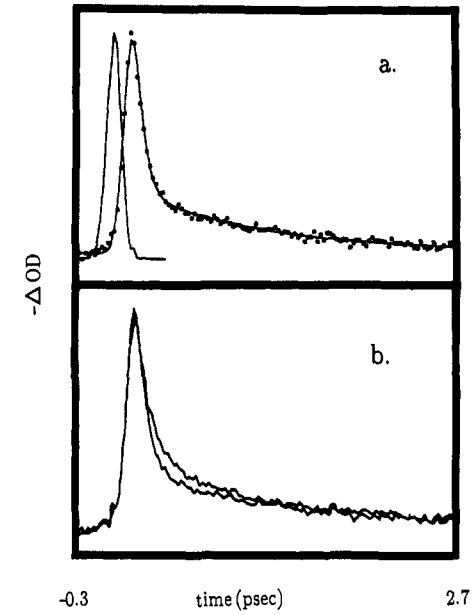


**Figure 2.** (a) The transient bleach signal of $(NH_3)_5Ru^{III}NCFe^{II}(CN)_5^-$ in $H_2O$ with pump and probe at 792 nm. The sharp peak at early time is the instrument response function (offset for visual clarity). The data (circles) is fit with the asymmetric curve which corresponds to a convolution of the instrument response function and three-exponential model for the decay. The fitted values are $\tau_1$ = 0.05 ps (86%), $\tau_2$ = 1.2 ps (12%), and $\tau_3 > 75$ ps (1.5%). We assign the second component to reverse electron transfer, although some of the faster component may also reflect reverse electron transfer (see text for details). (b) A comparison of the transient signal in $H_2O$ (lower trace) and $D_2O$ (upper trace).

We have collected resonance Raman data on RuFe and analyzed it within the harmonic approximation to yield the coordinate displacements and the vibrational fundamental frequencies[13] as shown in Table I. From the displacements and frequencies, a reorganization energy $\lambda_i$ for each $i$th mode can be estimated. The total vibrational reorganization energy is $\lambda_{vib} = \Sigma\lambda_i \simeq 3200\ cm^{-1}$. The solvent reorganization energy can be estimated to be $\lambda_{solv} \simeq 2400\ cm^{-1}$. (See ref 12 for more details.) $\lambda_{vib}$ is identified with

(9) Vogler, A.; Kisslinger, J. *J. Am. Chem. Soc.* **1982**, *104*, 2311.
(10) Burewicz, A. Haim, A. *Inorg. Chem.* **1988**, *27*, 1611.
(11) To avoid using electrochemical estimates of the driving force which include considerable approximations, we have estimated the driving force as follows. We first estimate $\lambda_{solv}$ using the Marcus[2] expression, $\lambda_{solv,theo} = e^2(1/2r_1 + 1/2r_2 + 1/d)(1/D - 1/D_{static})$, where $e$ is the charge transferred, $r_1$ = 4.4 Å, $r_2$ = 3.5 Å, $d$ = 5.1 Å, and the Peckar factor is 0.55. Then, recognizing that this expression may overestimate $\lambda_{solv}$, we assume that $\lambda_{solv} \simeq 0.6\lambda_{solv,theo}$ based on estimates from several better characterized systems. See for instance: Hupp, J. T.; Meyer, T. J. *Inorg. Chem.* **1987**, *26*, 2332. Creutz, C. *Inorg. Chem.* **1978**, *17*, 3723. Oh, D.; Boxer, S. G. *J. Am. Chem. Soc.* **1989**, *111*, 1130. Using $r_1$ = 4.4 Å, $r_2$ = 3.5 Å, and $d$ = 5.1 Å, we obtain $\lambda_{solv,theo} \simeq 3800\ cm^{-1}$. Thus $\lambda_{solv} \simeq 2400\ cm^{-1}$. This results in $\Delta G^\circ \simeq 4600\ cm^{-1}$. An alternative technique uses the electrochemical data[10] of the individual metal complexes to predict a driving force of $\simeq 3000\ cm^{-1}$. Then using this value, $\lambda_{vib}$ from the resonance Raman data, and $h\nu_{abs,max}$, one can then estimate $\lambda_{solv}$ as 4900 $cm^{-1}$. Incorporating the values from the electrochemically based calculation in a theoretical analysis analogous to that summarized in Table II, the Sumi–Marcus rate becomes single exponential, with $k_{ET,SM} \simeq 4.4 \times 10^{11}\ s^{-1}$. The Jortner/Bixon rate is nearly unchanged, $k_{ET,JB} \simeq 1.0 \times 10^{12}\ s^{-1}$. In this case, the Jortner/Bixon ET is a "normal regime" ET, and the similarity of the two Jortner/Bixon predicted rates results from several favorable Franck–Condon factors.

(12) Kjear, A. M.; Ulstrup, J. *J. Am. Chem. Soc.* **1987**, *109*, 1934.
(13) Heller, E. J. *Acc. Chem. Res.* **1981**, *14*, 368. Tannor, D.; Heller, E. *J. Chem. Phys.* **1982**, *77*, 202. Heller, E. J.; Sundberg, R. L.; Tannor, D. *J. Phys. Chem.* **1982**, *86*, 1822.

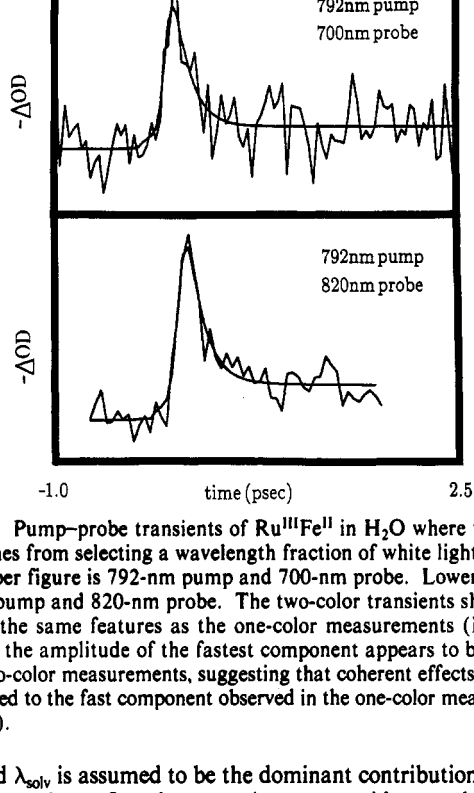


**Figure 3.** Pump–probe transients of $Ru^{III}Fe^{II}$ in $H_2O$ where the probe light comes from selecting a wavelength fraction of white light continuum. Upper figure is 792-nm pump and 700-nm probe. Lower figure is 792-nm pump and 820-nm probe. The two-color transients show qualitatively the same features as the one-color measurements (Figure 2) although the amplitude of the fastest component appears to be smaller in the two-color measurements, suggesting that coherent effects probably contributed to the fast component observed in the one-color measurement (see text).

$\lambda_{QM}$, and $\lambda_{solv}$ is assumed to be the dominant contribution to $\lambda_{class}$, i.e., $\lambda_{class} \simeq \lambda_{solv}$. In a later section we consider an alternative approximation for the decomposition of $\lambda$ into $\lambda_{solv}$ and $\lambda_{vib}$.

**Ultrafast Pump–Probe Spectroscopy.** Figure 2a shows a pump–probe, optical density transient for $Ru^{III}Fe^{II}$ in $H_2O$ at 293 K, where $\lambda_{pump} = \lambda_{probe} = 792$ nm. The upward direction in Figure 2 corresponds to a negative optical density, i.e., decreasing absorption or "bleach". The optical transient can be fit well by a convolution of a triexponential model decay $\Delta OD(t) = A_1 \exp(-t/\tau_1) + A_2 \exp(-t/\tau_2) + A_3 \exp(-t/\tau_3)$ and the experimental instrument response function. A typical set of parameters with the amplitudes represented as percentages is as follows: $\tau_1 = 0.05$ ps (86%), $\tau_2 = 1.2$ ps (12%), $\tau_3 > 75$ ps (1.5%). These parameters are not significantly dependent on laser power (varied by a factor of 5) or the concentration of $Ru^{III}Fe^{II}$ (varied over a factor of 10). Single-color ($\lambda_{pump} = \lambda_{probe}$) polarization measurements indicate that the relative amplitude of first component, $\tau_1$, changes by less than 50% when the probe polarization is rotated 90°. For the purpose of discussion we denote the three kinetic components as processes I, II, and III, in order of decreasing rate.

We have also detected the transient pump–probe signal ($\lambda_{pump} = 792$ nm) with $\lambda_{probe} = 820$ nm (Figure 3a) and, alternatively, $\lambda_{probe} = 700$ nm (Figure 3b). The signal to noise of these latter two transients is much less than the experiments in Figure 2 because the probe light for Figure 3 was continuum and has more intensity fluctuation than the 792-nm laser source which was used in the experiments in Figure 2. Nevertheless, the dynamics we observe at $\lambda_{probe} = 792$ nm are qualitatively similar to the dynamics at $\lambda_{probe} = 820$ nm and $\lambda_{probe} = 700$ nm within the marginal signal to noise of the measurements of Figure 3. The pulse-limited ($\tau \simeq 50$ fs) component I has a smaller (factor of $\simeq 2$) relative amplitude in the measurements with $\lambda_{pump} \neq \lambda_{probe}$, suggesting that component I may be partly due to a coherent artifact.[14] However, the facts that (i) component I is observed even when the probe wavelength is extensively detuned from the pump wavelength and (ii) component I shows weak polarization dependence suggest that a large portion of component I is due to an ultrafast component of $k_{ET}$.

The interpretation of component II is more straightforward because coherent artifacts are an unlikely complication at this time scale ($\tau \simeq 1$ ps vs $\simeq 0.1$ ps pulse width). We tentatively assign component II to direct ground-state recovery, i.e., ET, although more extensive, variable-wavelength pump–probe measurements are in progress to evaluate this assignment. The slowest kinetic process (component III) is assigned to an unresolvably slow decay of a small fraction (<10%) of the excited molecules due to an unassigned side reaction, such as from $Ru^{II}Fe^{III}$ to another excited electronic state of $Ru^{III}Fe^{II}$, which would subsequently relax (perhaps slowly) to ground-state $Ru^{III}Fe^{II}$.

We have also measured the pump–probe signal in $D_2O$ instead of $H_2O$; see Figure 2b. There is a clear diminution in the rate of absorption recovery. We note that when $Ru^{III}Fe^{II}$ is dissolved in $D_2O$ ammine protons may exchange with solvent deuterons. Further experiments are under way to examine the consequences of this exchange.

In conclusion, pump–probe measurements on the MMCT band of $Ru^{III}Fe^{II}$ show three apparent time scales for absorption recovery. The second component ($\tau_2 = 1.2$ ps) has been assigned to direct ET ($Ru^{II}Fe^{III} \rightarrow Ru^{III}Fe^{II}$), while the fastest process may be due partly to ET and partly to a coherent artifact. The experimental measurements, therefore, indicate that the rate of direct photoinduced ET falls in the range $10^{13}$–$10^{12}$ $s^{-1}$, depending on the extent to which component I is due to ET.

## Theoretical Predictions

Contemporary ET theory involves an explicit treatment of the recently recognized, important role of solvation dynamics in ET kinetics.[7,15-19] It is convenient to consider two specific theoretical models that treat the interplay of solvation dynamics and vibrational degrees of freedom, namely, the theory of Sumi and Marcus,[16a] which treats the vibrational modes classically, and the theory of Jortner and Bixon,[17] which involves a quantum mechanical model for the vibrations.

Both of these models involve a simple "Debye" model for the dynamics of the solvent coordinate involving a single relaxation time. Simulations on the self-exchange ET $Fe^{II}/Fe^{III}$ by Bader et al.[18] and related simulations in water[7] indicate that more complex solvation dynamics actually occur in aqueous environments. The impact of the complex solvation dynamics has been discussed by Hynes et al.[19] and others,[7] in terms of a frequency-dependent solvent friction formulation.

The theoretical treatment of Sumi/Marcus[16a] is based on a diffusive mechanism for the solvent coordinate. The actual ET event is assumed to occur along vibrational coordinates which are treated classically. A key element is the solvent coordinate dependent rate coefficient

$$k(x) = \nu_q \exp(-\Delta G^*(x)/k_bT) \quad (4)$$

where $\nu_q$ is the effective frequency factor and $\Delta G^*(x)$ is the $x$-dependent activation energy. For the reaction $Ru^{II}Fe^{III} \rightarrow Ru^{III}Fe^{II}$, $V_{el}$ is large enough to ensure that the adiabatic expression for $\nu_q$ is appropriate, as follows

$$\nu_q = (\sum_j \nu^2_j \lambda_i/\lambda_{vib})^{1/2} \simeq 1200 \text{ cm}^{-1} \quad (5)$$

(14) von Jena, A.; Lessing, H. E. *Appl. Phys.* **1979**, *19*, 131.

(15) Huang, J.-K.; Creighton, S.; King, G.; Whitney, D.; Warshel, A. *J. Chem. Phys.*, in press. Warshel, A. Chu, Z. T. *J. Chem. Phys.* **1990**, *93*, 4003.

(16) (a) Sumi, H.; Marcus, R. A. *J. Chem. Phys.* **1986**, *84*, 4894. (b) Nadler, W.; Marcus, R. A. *J. Chem. Phys.* **1987**, *86*, 3906.

(17) Jortner, J.; Bixon, M. *J. Chem. Phys.* **1988**, *88*, 167.

(18) Bader, J. S.; Chandler, D. *Chem. Phys. Lett.* **1989**, *157*, 501. Bader, J. S.; Kuharski, R. A.; Chandler, D. *J. Chem. Phys.* **1990**, *93*, 230.

(19) van der Zwan, G.; Hynes, J. T. *J. Phys. Chem.* **1985**, *89*, 4181. Hynes, J. T. *J. Phys. Chem.* **1986**, *90*, 3701. Ciccotti, G.; Ferrario, M.; Hynes, J. T.; Kapral, R. *J. Chem. Phys.* **1990**, *93*, 7137.

(20) $k_{ET,JB(mod)}$ exceeds $1/\langle\tau_s\rangle$. This result, however, may be unphysical because $k_{ET}$ should not significantly exceed the rate of diffusion ($k_D \simeq \langle\tau_s\rangle^{-1} \simeq 2 \times 10^{12}$ $s^{-1}$) from the bottom of the well to the lowest energy avoided crossing ($0 \rightarrow 0$). Apparently, the generalized Jortner/Bixon model overestimates the total rate because it simply adds partial rates of individual channels, which is not physically correct since the various adiabatic channels should effectively "kinetically interfere". Instead, a more fundamental theoretical approach is required. However, such an approach is computationally intensive and beyond the scope of this paper.

TABLE II: Predicted Electron-Transfer Rates for $Ru^{II}Fe^{III} \rightarrow Ru^{III}Fe^{II}$, with Associated Parameters[a]

| theory | $k_{ET}$ | $\lambda_{class}$ | $\lambda_{sol}$ | $\lambda_{class,vib}$ | $\lambda_{QM}$ | $\nu_{QM}$ | $\langle\tau_s\rangle^{-1}$ |
|---|---|---|---|---|---|---|---|
| Sumi/Marcus | 10, 5[b] | 5600 | 2400 | 3200 | | [c] | 1.7[f] |
| Jortner/Bixon | 1.2 | 2400 | 2400 | | 3200 | 1225 | 1.7 |
| Sumi/Marcus (modified) | 1.1, 0.8[b] | 3200 | 2400 | 800 | | [d] | 1.7 |
| Jortner/Bixon (modified) | 8.0 | 1600 | 1600 | | | [e] | 1.7 |

[a] All rates are in units of $10^{12}$ $s^{-1}$. Reorganization energies $\lambda$ are in units of $cm^{-1}$. [b] Two characteristic rates result from this analysis; see text for further details. [c] The average phonon frequency $\nu$ enters into the Sumi–Marcus expression (eq 4.6 in ref 16a) which is used as part of estimating $k_{ET,SM}$, i.e., $\nu = \nu_q(\lambda_{class,vib}/\lambda_{class})^{1/2} = 2.9 \times 10^{13}$ $s^{-1}$. [d] As in c, except $\nu = 3.4 \times 10^{13}$ $s^{-1}$. [e] In this analysis there are two quantum modes, one intramolecular and one solvent. Their frequencies and reorganization energies are $\nu_{qm} = 1225$ $cm^{-1}$ ($\lambda_{qm} = 3200$ $cm^{-1}$) and $\nu_{qm,solv} = 400$ $cm^{-1}$ ($\lambda_{qm,solv} = 800$ $cm^{-1}$), respectively. See text for further details. [f] $\langle\tau_s\rangle$ is the average solvation time as measured by using the time-dependent Stokes shift method using coumarin 343 in water; see ref 5.

where $\lambda_{vib}$ is the total vibrational reorganization energy and the values in Table I have been used in eq 5. The remaining necessary parameters are the solvent reorganization energy $\lambda_{solv}$, the driving force $\Delta G°$, and the average solvent relaxation time $\langle\tau_s\rangle$, which are listed in Table II.

Employing these parameters, the Sumi/Marcus prediction for the rate, $k_{ET,SM}$ (see Table II), is obtained by use of the numerical results in Figures 2 and 3 of ref 16a. $k_{ET,SM}$ is multiexponential, reflecting (i) a rapid ET that occurs from an already favorable solvent distribution and (ii) a slower ET influenced by solvent diffusion.

In contrast to the Sumi/Marcus model, the Jortner/Bixon[17] approach treats the vibrational coordinates quantum mechanically. In particular, a single vibrational mode is employed, and the total ET rate from $v = 0$ of the reactant to all possible vibrational levels $n$ of the product is given by

$$k_{ET,JB} = \sum_n k_{NA}^{on}/(1 + \mathcal{H}_A^{(n)}) \quad (6)$$

where $n$ refers to the quantum level of the high-frequency accepting mode in the product state. $k_{NA}^{on}$ is the nonadiabatic rate constant for each vibronic channel, i.e.

$$k_{NA}^{on} = \frac{2\pi V_n^2}{\hbar(4\pi\lambda_{solv}k_BT)^{1/2}} \exp(-\Delta G^{\ddagger}_{on}/k_bT) \quad (7)$$

where $V_n$ is the Franck–Condon "dressed" matrix element, and $\Delta G^{\ddagger}_{on}$ is the effective activation energy for the $0 \rightarrow n$ channel. The adiabicity parameter $\mathcal{H}_A$ in eq 6 is given as $\mathcal{H}_A = 4\pi V_n^2 \cdot \langle\tau_s\rangle/\hbar\lambda_{solv}$, where we have substituted $\langle\tau_s\rangle$, the experimentally measured average solvation time, for $\tau_l$, the continuum estimate for the solvation time which was used by Jortner and Bixon.

The Jortner/Bixon model employs a single effective vibrational degree of freedom. In order to invoke this theory, we use the average vibration frequency estimated by eq 5 and the reorganization energy in that "average" mode to estimate the Franck–Condon factors.[13,17] The Jortner/Bixon rate, $k_{ET,JB}$, employing this effective vibrational mode is given in Table II. $k_{ET,JB}$ is dominated by the third vibronic channel, $0 \rightarrow 2$, which is predicted to be solvent controlled.

The Sumi–Marcus analysis, which includes all reorganization energy in calculating $\Delta G^*$, results in a "normal regime", nearly "barrierless regime" ET. Due to the magnitude of $\Delta G°$, the partitioning of vibrational reorganization energy into quantal degrees of freedom results in the Jortner/Bixon "inverted regime" prediction, which then depends on quantal degrees of freedom to reduce the effective activation barrier to enhance $k_{ET}$.

**Comparison of Theory and Experiment and Frequency-Dependent Solvent Friction.** It is noteworthy that the experimental results agree with both theoretical results to within a factor of roughly 4, generally supporting the validity of these models. Both models point out the importance of the vibrational coordinates, though in surprisingly different ways. In the Sumi/Marcus case, vibrational frequencies enter most significantly in the preexponential factor, $\nu_q$. In the Jortner/Bixon case, quantal vibrations serve to reduce the effective activation barrier. However, the enhancement of $k_{ET,JB}$ due to quantal effects is not as large as the $10^5$ "quantal" enhancement recently observed in the strongly "inverted regime" ET of betaine-30.[8a]

Both theoretical models predict that the ET rate is diminished by dynamic solvent effects. Indeed, the predicted rate according to the Jortner/Bixon model is close to $1/\langle\tau_s\rangle$, which implies that the ET kinetics may depend on the initial distribution along the reaction coordinate. Because the ET reaction in this paper is initiated by ultrafast laser excitation, the solvent coordinate is actually prepared in the displaced configuration, rather than the equilibrated configuration in $Ru^{II}Fe^{III}$ which is more consistent with the theoretical models. Nevertheless, the Jortner/Bixon prediction that $k_{ET} \simeq \langle\tau_s\rangle^{-1}$ should still apply even though solvent diffusion is occurring from the "high-energy side" of the avoided crossing; see Figure 1.

It should be emphasized that the Sumi/Marcus and Jortner/Bixon predictions made above are based on the assumption that the solvent coordinate relaxation is overdamped and is manifested by a single relaxation time. However, molecular dynamics simulations of solvation of $Fe^{II}/Fe^{III}$ in water,[18] and related simulations of solvation in water,[7] reveal a complex dynamical behavior indicative of inertial motion at early times (<50 fs) involving librations of water and diffusional motion at later times. Although the transient Stokes shift measurements on polar fluorescent probes in water measured a distribution of solvation components (or frequency-dependent solvent friction),[7] the initial, faster components are apparently too rapid to resolve by existing transient emission methods.[8]

Hynes and co-workers[19] have shown that frequency-dependent solvent friction can dramatically alter theoretical predictions of $k_{ET}$. In order to estimate roughly the role of frequency-dependent solvent friction in the case of $Ru^{II}Fe^{III}$, we have separated the solvent coordinate into a low-frequency (lf) overdamped mode and a high-frequency (hf) inertial mode which we model classically and quantum mechanically, respectively. The parameters are as follows: $\lambda_{solv,cl}^{(lf)} = 1600$ $cm^{-1}$, $\lambda_{solv,qm}^{(hf)} = 800$ $cm^{-1}$, and $\nu_{solv,qm}^{(hf)} = 400$ $cm^{-1}$. These values have been estimated from the power spectrum of the solvation dynamics of the bulk solvent in Chandler and co-workers's[18] simulation of solvation dynamics of aqueous $Fe^{II}/Fe^{III}$. Our treatment thus includes two quantum modes (one intramolecular and one solvent) and one classical solvent mode.

The Jortner/Bixon prediction using this modified treatment of the solvent is denoted by $k_{ET,JB(mod)}$ in Table II. Note that this result is faster than $k_{ET,JB}$ because the effective solvent barrier has been reduced by partitioning some of the solvent reorganization energy to a quantal mode and allowing combination $(v_1,v_2) \rightarrow (v_1',v_2')$ vibronic transitions.

*Acknowledgment.* P.F.B. acknowledges the National Science Foundation and Office of Naval Research for partial support of this research. J.T.H. acknowledges support from the U.S. Department of Energy, Office of Energy Research, Division of Chemical Sciences (Grant DE-FGO2-87ER13808), and the Alfred P. Sloan Foundation.